microLife, 2024, **5**, uqae020
DOI: 10.1093/femsml/uqae020
Advance access publication date: 4 October 2024
Research Article

Inferring bacterial interspecific interactions from microcolony growth expansion

Tania Miguel Trabajo[1], Isaline Guex[1,2], Manupriyam Dubey[1], Elvire Sarton-Lohéac[1], Helena Todorov[1], Xavier Richard[2], Christian Mazza[2], Jan Roelof van der Meer[1,*]

[1]Department of Fundamental Microbiology, University of Lausanne, Batiment Biophore, Quartier UNIL-Sorge, 1015 Lausanne, Switzerland
[2]Department of Mathematics, University of Fribourg, 1700 Fribourg, Switzerland
*Corresponding author. Department of Fundamental Microbiology, University of Lausanne, 1015 Lausanne, Switzerland. E-mail: Janroelof.vandermeer@unil.ch
Editor: Axel Brakhage
Reviewers: Leo Eberl, Victor de Lorenzo, Paul Rainey & Yuya Karita

Abstract

Bacterial species interactions significantly shape growth and behavior in communities, determining the emergence of community functions. Typically, these interactions are studied through bulk population measurements, overlooking the role of cell-to-cell variability and spatial context. This study uses real-time surface growth measurements of thousands of sparsely positioned microcolonies to investigate interactions and kinetic variations in monocultures and cocultures of *Pseudomonas putida* and *P. veronii* under substrate competition (succinate) or substrate independence (d-mannitol and putrescine). In monoculture, microcolonies exhibited expected substrate-dependent expansion rates, but individual colony sizes were affected by founder cell density, spatial positioning, growth rates, and lag times. In coculture, substrate competition favored *P. putida*, but unexpectedly, reduced the maximum growth rates of both species. In contrast, 10% of *P. veronii* microcolonies under competition grew larger than expected, likely due to founder cell phenotypic variation and stochastic spatial positioning. These effects were alleviated under substrate independence. A linear relationship between founder cell ratios and final colony area ratios in local neighborhoods (6.5–65 µm radius) was observed in coculture, with its slope reflecting interaction type and strength. Measured slopes in the *P. putida* to *P. veronii* biomass ratio under competition were one-third reduced compared to kinetic predictions using a cell-agent growth model, which exometabolite analysis and simulations suggested may be due to metabolite cross-feeding or inhibitory compound production. This indicates additional factors beyond inherent monoculture growth kinetics driving spatial interactions. Overall, the study demonstrates how microcolony growth experiments offer valuable insights into bacterial interactions, from local to community-level dynamics.

Keywords: growth kinetics; *Pseudomonas putida*; *Pseudomonas veronii*; substrate competition; phenotypic heterogeneity; spatiality

Introduction

Understanding how interactions between microbial cells of different species shape the formation and functioning of multispecies communities, remains a long coveted goal in microbial ecology (Faust and Raes 2012, Coyte et al. 2015, Zelezniak et al. 2015, Kehe et al. 2021, Schäfer et al. 2023), and multiple methods to measure interspecific interactions have been put forward (Pacheco et al. 2022). Depending on the data type and the theoretical framework, interaction concepts have been based on, for example, species co-occurrence networks (Faust and Raes 2012, Widder et al. 2022), machine-learned community compositional patterns (Emmenegger et al. 2023), resource utilization (Piccardi et al. 2019, Rodríguez Amor and Dal Bello 2019, Dal Bello et al. 2021, Nestor et al. 2023) and nutrient niche overlap predictions (Schäfer et al. 2023), metabolite exchange (Zelezniak et al. 2015, Pacheco et al. 2019, Kehe et al. 2021), or growth expansion patterns (Momeni et al. 2013, Goldschmidt et al. 2017, Borer et al. 2020), and even on cell–cell contact secretion systems (Basler et al. 2013, Niggli et al. 2021). In addition, species interactions can evolve under spatially structured conditions, leading to diversification (Rainey and Rainey 2003) and increased cooperation (Hansen et al. 2007). One of the difficulties to extrapolate from different interaction levels to community formation, is their integration across spatial scales and time, and their embedment in appropriate growth kinetic frameworks (van den Berg et al. 2022). Connecting here to classical Monod-type growth kinetics would make sense, given its prevalence and acceptance in the context of pure culture physiology, and recent adaptations to the level of multispecies growth (Goldford et al. 2018, Liao et al. 2020, Dal Bello et al. 2021, van den Berg et al. 2022, Guex et al. 2023). However, co- or multispecies culture data adaptable to multispecies Monod-type growth kinetic frameworks are still scarce, as one needs appropriate parameter values for monoculture growth rates and yields, their dependencies on nutrient conditions, starting ratios, and their variability under influence of emerging interspecific interactions in cocultures. To achieve this, we develop here a scalable methodology to extract kinetic and interaction parameters from real-time spatial microcolony growth patterns in mono- and cocultures, based on previous pure culture tools in the area of environmental, food, and medical microbiology (Reinhard and van der Meer 2010, Eijlander and Kuipers 2013, Koutsoumanis and Lianou 2013, Nghe et al. 2013, Jung and Lee 2016).

In contrast to growth kinetic and interaction measurements for two or more species in mixed liquid (suspended) cultures, real-time microcolony growth measurements can differentiate species by their spatial position and measure individual growth

Received 16 September 2024; **accepted** 3 October 2024

kinetics from colony expansion and final colony sizes. By placing dividing cells on the surface at start within a ca. 10–50 µm range, substrate and metabolite diffusion allow metabolic interactions to emerge. Quantifying growth and interactions at microcolony level would have the additional advantage of maintaining similar spatial scales that many bacterial cells face in natural, heterogeneous habitats, and under resource-diffusion limited growth conditions. In the context of unsaturated soil, for example, microbial growth habitats are characterized by small water-filled pockets, pores, and water-film covered surfaces (Tecon and Or 2017). It has been estimated that the majority of cell clusters in unsaturated soils have fewer than 100 cells (Bickel and Or 2023), with intercell distances averaging between 10 and 100 µm (Raynaud and Nunan 2014). Interspecific interactions are, therefore, also expected to emerge across short distances, with cells, potentially, going only through short growth cycles as a result of limited carbon, water, and space.

The objectives of this research were to expand a microcolony growth framework from single pure to mixed cultures, such that relevant kinetic parameters can be extracted of the individual species in the mixture and emerging interspecific interactions can be quantified across relevant local scales (10–100 µm intercell distances). Our set-up consists of microscopic growth chambers with cells growing on miniature nutrient surfaces (Reinhard and van der Meer 2010, 2014) that can be operated under long incubation times (2–4 days), enabling real-time microscopy of all growth phases from individual founder cells to mature microcolonies (i.e. lag times, exponential growth, and stationary phase). To benchmark the concept, we deployed two fluorescently labeled soil bacteria: *Pseudomonas veronii* (Morales et al. 2016) and *P. putida* (Zylstra and Gibson 1989), and quantified growth in individual mono- and cocultures under both competitive (i.e. same primary substrate or shared metabolites) or substrate independence conditions (i.e. each species has its own unique substrate). In previous work, we had tested both strains in mono- or coculture homogenous liquid culture conditions and different starting ratios, showing that *P. putida* outcompetes *P. veronii* under single substrate competition as expected from growth kinetic differences, but with more than expected metabolite sharing (Guex et al. 2023). In addition to the microcolony growth experiments, we also developed an individual cell-agent model based on Monod growth under substrate-diffusion conditions and with inclusion of interspecific interactions (Guex et al. 2023), that we parametrized using the empirical kinetic data in order to understand growth and interaction effects both at the scale of local individual microcolonies, and at the level of the community as a whole (the ensemble of all microcolonies on the growth surface). Our results indicate good agreement of averaged microcolony growth in mono- and cocultures and bulk population interaction measurements, with local (13–40 µm diameter) neighborhood analysis, but surprising effects of variations in single (founder) cell kinetic parameters on the local reproductive success. Contrary to the typical influence of interactions on species yields, we find that competitive interactions can also reduce maximum specific growth rates of either partner. Although shown here for a defined coculture, the same microscopic growth platform is scalable to more complex mixed cultures.

Materials and methods

Study system design for interspecific interaction measurements from microcolony growth

We deployed a closed sterile microscopy chamber with a 1-mm-thin agarose-solidified disk ("agarose patch;" Fig. 1A), containing low carbon substrate concentrations (1 mM, to avoid multilayered growth), onto which individual cells are randomly and sparsely seeded (Reinhard and van der Meer 2014). Cell division into microcolonies is imaged and recorded by time-lapse epifluorescence microscopy (Fig. 1A), from which colony expansion rates, lag times, final colony size area, colony distances, and other relevant parameters are extracted and compared between individual mono- and coculture incubations. The system was benchmarked with *Pseudomonas putida* (Ppu) and *P. veronii* (Pve), cultured either under conditions of (assumed) direct substrate competition or substrate independence. To induce substrate competition, we added succinate to the agarose patch, whereas substrate independence was generated by adding both D-mannitol, as a specific substrate for Pve, and putrescine for Ppu (Guex et al. 2023). Local biomass formation (by microscopy) for either strain alone or in coculture was compared to bulk yields across the whole patch, by washing cells from the surfaces at the end of the experiment and counting either species by flow cytometry on the basis of its fluorescent marker.

Bacterial strains and preparation of founder cell cultures

Ppu F1 (Zylstra and Gibson 1989), was genetically labeled with a single copy mini-Tn5 insertion (Martinez-Garcia et al. 2011) constitutively expressing enhanced green fluorescent protein (eGFP) under the control of the ICE*clc*-promoter P_{circ} (Sentchilo et al. 2003) and containing a gene for kanamycin resistance. Pve 1YdBTEX2 (Morales et al. 2016) was labeled with a single copy mini-Tn*7* insertion constitutively expressing mCherry under the control of the P_{tac} promoter and providing gentamicin resistance (Rochat et al. 2010). Cultures were stocked at –80°C in 15% v/v glycerol and regrown for each experiment on nutrient agar medium (Oxoid CM 0067) with the appropriate antibiotics to obtain individual colonies. A single fresh colony was then precultured in liquid 21C minimal medium without vitamins (MM) (Gerhardt et al. 1981) supplemented with 5 mM of the carbon source to be tested in the patch, with the appropriate antibiotic included, and incubated at 30°C with rotary shaking (160 rpm). Cells were harvested from a 2-ml aliquot sampled from exponentially growing (culture density of $OD_{600} = 0.8$) or from stationary phase cultures. The aliquot was centrifuged for 2 min at 13 000 rpm in a Heraeus Fresco 21 microfuge (Thermo Scientific) at room temperature. The supernatant was decanted, and the cell pellet was resuspended in 1 ml MM (without carbon source). This procedure was repeated twice more. After the final resuspension, the culture turbidity was again measured, and suspensions were diluted with MM to an OD_{600} of 0.07 for Ppu and 0.11 for Pve. Cell numbers were quantified further by flow cytometry (see below). These suspensions were then used directly for monoculture patch seeding or mixed in a 1:1 v/v ratio to produce cocultures with approximately equal founder cell numbers (seeding density details for each experiment in Table S1).

Preparation of microcolony growth surfaces

Molten agarose solution was prepared with 10 g l^{-1} UltraPure™ Agarose (Invitrogen, 16500–100) in MM, to which the desired carbon source was added while the agarose mixture was still liquid at 45°C. Stocks of individual carbon sources (succinate, 490 mM; putrescine, 33 mM; and D-mannitol, 150 mM) were prepared by weighing from the pure substance (Sigma Aldrich) in ultrapure water, which was sterilized by passing through a 0.2-µm membrane filter (ClearLine, 037 044). Carbon substrates were diluted in the agarose solution to achieve final concentrations of: 0.01, 0.05, 0.5, 1, or 5 mM (for succinate); or 0.66 mM for putrescine plus 1 mM

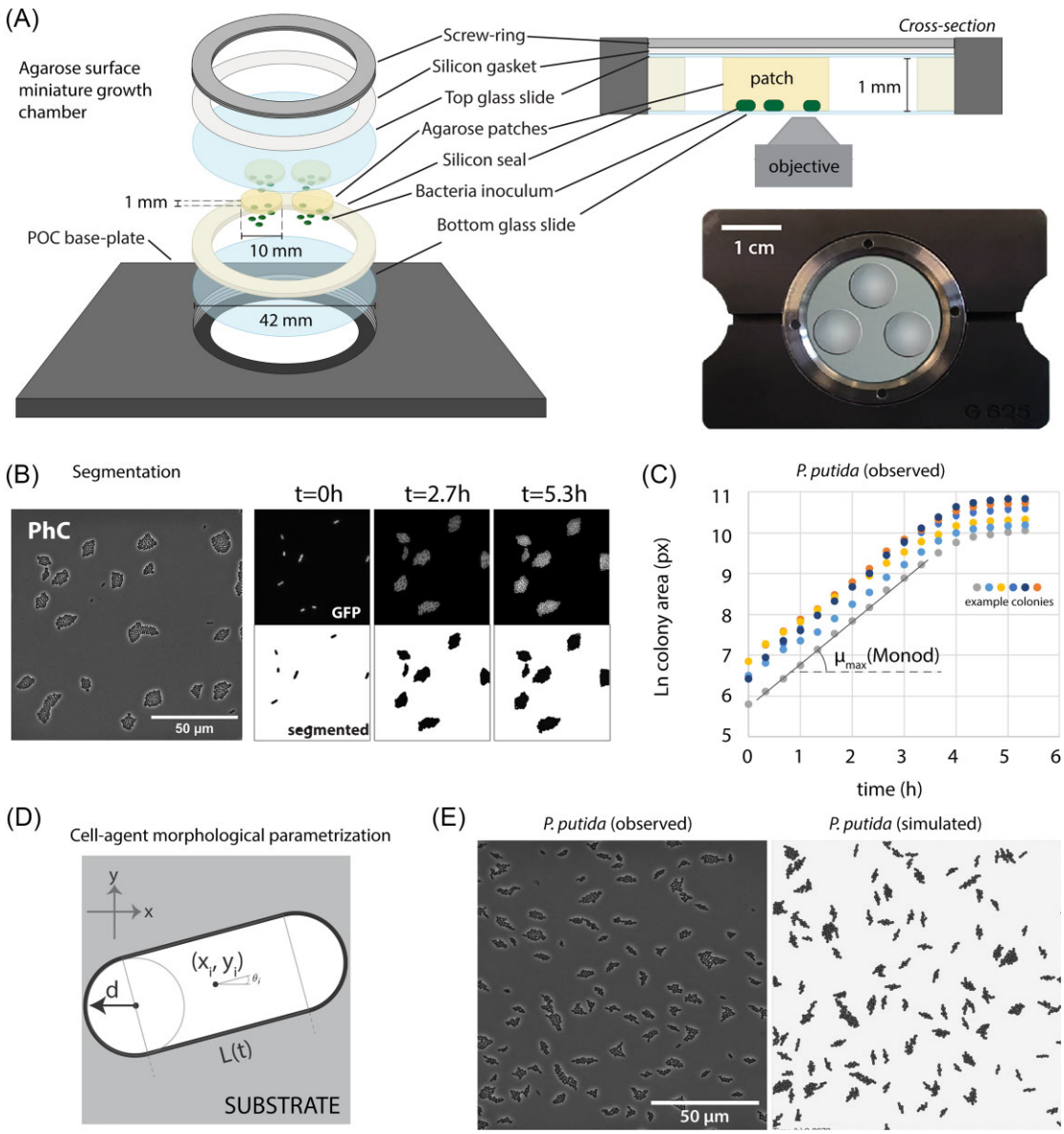

Figure 1. Set-up and principle of the microcolony growth expansion experiments. (A) Closed microcolony growth chamber to incubate the agarose patches (ø 10 mm, 1 mm thick) and the surface-deposited cells in inverse orientation for real-time epifluorescence microscopy. (B) Example of an imaged surface area with Ppu microcolonies in phase-contrast (PhC); epifluorescence snapshots (GFP) taken at difference time points (0, 2.7, and 5.3 h) and the resulting colony segmentation. (C) Deduction of maximum specific growth rates as the slope from ln-transformed segmented microcolony areas (colors correspond to individual microcolonies) over time. (D) Cell-agent used for the Monod-based growth model, assuming cylindrical cells with length $L(t)$ and poles with half-circle radius d, expanding and in x, y direction on the surface substrate. (E) Comparison of observed (phase-contrast) and simulated Ppu microcolonies at the same seeding positions and incubation times.

for D-mannitol (i.e. to have equal C-molarity for the independence scenario). Agarose without any added carbon substrate served as a control for background growth.

A volume of 1.5 ml of agarose–carbon substrate solution at 45°C was poured on a circular 42-mm diameter and 0.37-mm thick glass slide (H. Saur Laborbedarf, Germany) enclosed with a 1-mm thick silicon ring (Fig. 1A; Fig. S1A) (Reinhard and van der Meer 2010). Immediately after pouring, a second glass slide was placed on top to give the patch the desired thickness. After 5 min solidification, the top slide was gently removed (Fig. S1B) and multiple 1-cm ø circular disks were punched from the solid agarose using a steel hole puncher previously sterilized with the flame (e.g. hammer-driven hole punch, McMaster-Carr, Cleveland, OH, USA, catalog number 3418A1; Fig. S1C). Circular disks were arranged on a new round glass slide (maximum four per slide; Fig. 1A). An aliquot of 10 µl of diluted founder cell suspension (either mono- or coculture mixture), was then carefully pipetted on each surface and spread homogenously, and dried for 10 min in a laminar sterile flow hood at 21°C (Fig. S1D). The slide with patches was turned upside down on a new clean round glass coverslip with a separation silicon ring of 1 mm thickness, which was mounted in a sterilized black anodized chamber (Perfusion Open and Close - POC chamber; H. Saur Laborbedarf). A further 0.5-mm thick silicon gasket was placed on the top glass coverslip, before closing the chamber with a screw ring (without putting pressure on the slide). In the final setup (Fig. 1A), cells are caught in between the lower cover slip and the agarose surface, whereas the top of the agarose touches the upper coverslip (i.e. no air space in between to

avoid condensation droplets; Fig. 1A). The remainder of the chamber has ambient air that diffuses into the patches from the sides.

Time-lapse imaging of microcolony growth

Microscope chambers were mounted (cells facing down) and incubated on a Nikon ECLIPSE Ti Series inverted microscope coupled with a Hamamatsu C11440 22CU camera and a Nikon CFI Plan Apo Lambda 100× oil objective (1.45 numerical aperture, 1000× final magnification). The temperature was kept between 22°C and 24°C. Time-lapse programming was controlled by a script in MicroManager Studio version 1.4.23. Images in phase contrast, GFP or mCherry fluorescence were taken every 20 min, with exposure times of 30 ms, 50 ms, and 100 ms, respectively, and using a 4% power-set pE-100 LED illumination system from CoolLED. Imaging positions (between 8 and 10 per patch) were defined randomly at the start, but within a 3-mm radius of the patch center to avoid edge effects, and then kept for the remainder of the experiment. The total duration of the growth varied between experiments, from 12 h (in case of imaging only exponential growth) to 72 h (capturing stationary phase microcolonies). Images (2048 × 2048 pixels) were saved as 16-bit .tif files for each channel, per position and per time point. Images for display were cropped to the necessary size using Adobe Photoshop (version 2022), and saved at 300 dpi resolution before placing.

Image analysis and extraction of growth kinetic parameters

Microcolony growth was extracted from the fluorescent time-lapse image files, which were processed in a custom-made Python script (version 3.8.3) through a Jupyter Notebook (version 6.0.3). Colonies were segmented at each time step on the fluorescent images using the Otsu algorithm with a variable threshold that adapts to every frame. We noticed that the segmented fluorescent area of stationary phase microcolonies of Pve increased slightly despite not showing any further cell division, which we attribute to continued expression of the fluorescent protein and cells becoming brighter. This effect was not further corrected but does not influence colony expansion rate measurements. Segmented areas were stored as individual objects (in pixels), aligned across images, and then overlaid from a complete time-series in order to extract colony area expansion rates (Fig. 1B and C). Nondividing single cells (objects with the same size at the beginning and at the end of the time-lapse) were removed by filtering, but single elongating cells were included (even if eventually they did not divide). Microcolonies positioned near the image edges (within 200 px from the border) were removed to avoid taking incomplete microcolonies into account.

Maximum colony expansion rates were calculated from the exponential growth phase as the mean of moving linear slopes of ln-transformed colony areas versus time, including at least five consecutive time points and only slopes with an $r^2 > 0.99$. Colonies with starting areas <150 px (which can be the result of faulty image overlays) were corrected to the minimum cell size (=120 px for Ppu and 150 px for Pve) before calculating ln-transformed slopes. Since colony area is a proxy for cell biomass, the maximum colony expansion rate r from the ln-transformed areas was taken as the μ_{max} of biomass growth of the respective colony.

Flow cytometry quantification of total cell numbers

To quantify the final (combined) cell numbers of either strain growing on the agarose patches, the cells were washed from the surface at the end of the experiment by dismounting the POC chamber, flooding each individual patch with 2 ml MM, and pipetting repeatedly to resuspend the cells. This suspension was subsequently 10-fold serially diluted in MM and aspired on a NovoCyte Flow cytometer (OMNI Life Science Agilent) at a flow rate of 14 µl min^{-1} and a total analysed volume of 15 µl. Counts in diluted samples were retained for the final abundance calculation if less than 10^7 events. Strains were gated based on their specific fluorescence using the NovoExpress software (version 1.4.1). GFP was measured with the instrument's FITC channel (excitation at 488 nm and emission/detection at 530 nm), whereas mCherry fluorescence was detected in the PE-Texas Red channel (561 and 615 nm).

Individual cell-agent surface growth model

To better understand the underlaying factors causing growth kinetic variations in mono and cocultures, we simulated microcolony growth on the agarose patch in an agent-based surface growth kinetic model with a continuum field description of chemical reaction and transport (Fig. 1D and E; Supplementary methods). The model simulates microcolony growth in 2D from dividing single cell agents as a function of substrate diffusion, uptake, and metabolism, and of excretion/utilization of metabolic by- or end-products. Individual cell-agents (with volumes similar to actual Ppu or Pve cells) are positioned on a grid surface with similar dimensions as the experimentally imaged surface areas (134 × 134 μm^2). The number and positions of founder cell agents in the model can be chosen according to experimentally observed cell densities and geometric cell center positions, or randomly. Cell-agents are given inherent growth kinetic properties (i.e. μ_{max}, K_s and yield) by sampling from experimental data or by some *a priori* definition, allowing cell-to-cell variations and/or individual lag times (i.e. before the onset of growth and division). The model then assumes substrate to biomass conversion following Monod growth and yield, which is translated into cell elongation and division. Simulations calculate changes in resources, metabolites, cell-agent biomass, and positions for each time step Δt (corresponding to ca. 0.72 s) and per volumetric box of 3.7 pL in the surface grid. Molecular diffusion across boxes is recalculated after every time step. Cell agents reposition after each time interval as a function of cell pushing and shoving when forming microcolonies (Angeles-Martinez and Hatzimanikatis 2021). After the preset simulation time (typically, 10–20 h, or 50 000–100 000 time steps), the final attained individual microcolony biomasses are quantified as the descent of each positioned cell-agent, and individual microcolony growth rates are fitted from biomass-over-time increases. Users can vary the concentration of resources in the model, the production rates of metabolites, and run different interaction scenarios (e.g. see Supplementary data simulations).

To simulate interspecific interactions, we varied production and consumption rates of byproducts, assuming, for simplicity, byproduct "groups;" as proposed in Guex et al. (2023). The influence of mutual or cross-wise utilization of excreted byproducts was then tested by varying the μ fraction attributed to the main substrate and to the byproducts, under the restriction that the total μ cannot surpass its experimentally observed value (Supplementary data simulations). To plot simulations and compare to microscopy images, the simulated cell-agent positions and areas across the surface grid at 20 min intervals were saved as .tif files and segmented using the Python script described above. The cell-agent model was entirely coded in MATLAB (version 2021b, MathWorks Inc).

Metabolite analysis in liquid culture

To characterize appearing metabolites during growth of either species in mono- or coculture, we grew Pve and Ppu in liquid MM with 10 mM succinate in Erlenmeyer flasks (500 ml with 100 ml culture, incubated at 30°C and 120 rpm rotary movement), and then swapped the cells at mid-exponential phase to continue growing in either their own culture medium or that of the other species. Individual monocultures were grown in biological triplicates to mid-exponential phase (3–6 h after inoculation, measured by culture turbidity—OD_{600}, using a Ultrospec 500 pro spectrophotometer from Amersham Biosciences), after which 90 ml were removed and centrifuged to recover the cells. The supernatant was decanted without disturbing the cell pellet and then further purified from cells by passing over a 0.2-µm membrane filter (ClearLine, 037044). The cell pellet was carefully resuspended in 2 ml sterile saline solution (0.9% NaCl) and its turbidity was measured. The cell-free supernatant was divided in equal volumes in two new sterile Erlenmeyer flasks, one of which was inoculated with its own resuspended cell pellet; the other with the resuspended cell pellet from the other species; both targeting a starting OD of 0.005. The cultures were then again incubated as before, and their growth was followed by spectrophotometry.

Aliquots (1.5 ml) for liquid chromatography–mass spectrometry (LC–MS) analysis were taken at the start (i.e. uninoculated medium); the mid-exponential phase (i.e. the filtered supernatants before swapping), and at the end of the incubations (i.e. swapped cultures). All samples were purified by filtering across a 0.2–µm membrane filter, then snap-frozen in liquid nitrogen, and stored at –80°C until analysed by targeted LC–MS (Agilent 6495 LC–MS QqQ system, conducted at the University of Lausanne, Metabolomics Unit). Compound abundances are reported as their mean peak areas across replicates.

Statistics

Basic distribution parameters (median, mean, standard deviation, standard error, coefficient of variation, and percentiles) were calculated using respective functions in *R studio* or MATLAB (version 2021b, MathWorks Inc.). Pearson and Spearman correlations were inferred using the *ggplot* and *ggstatsplot R*-packages, or MATLAB's *corr* function. T-tests were two-sided and unpaired, as implemented in MATLAB's *ttest2* function. The Monod substrate correlation was nonlinearly fitted with 95% confidence boundaries on the general function $a * (x/(b + x))$ using MATLAB's *fit* algorithm. Linear regression was conducted using the *polyfit* function in MATLAB, and outliers for the 20-µm neighborhood were categorized as being above 3 × SD of the residual variation of the regression at 65-µm neighborhood radius. Metabolites were considered statistically significantly different between Ppu and Pve their own and swapped supernatants if the Benjamin–Hochberg multiple testing adjusted P-value < .05.

Results

Extracting growth rates from microcolony area expansion in time-lapse microscopy

To extract kinetic and interaction parameters, we followed positions and real-time formation of microcolonies from individual cells of mono- or cocultures of Ppu and Pve, sparsely seeded on the surface of an agarose patch (1 mm thick and 1 cm diameter). The patch is embedded in a closed microscopy chamber under inclusion of air (Fig. 1A) (Reinhard and van der Meer 2014). The agarose contains a limiting amount of substrates to control the extent of colony growth (while acknowledging that the agarose itself also provides some carbon and nutrients for growth—see below). The agarose patches provide the cells with a solid surface to form microcolonies while preserving the diffusion rates of substrate molecules and metabolites close to that in liquid. Dividing cells will expand primarily in the two-dimensional plane, because they are enclosed between the agarose surface and the glass coverslip, facilitating imaging (Fig. 1A). By reducing the amount of primary carbon substrate or increasing the density of founder cells on the patch, the number of divisions per cell is limited and we observed that the colonization of the surface remains restricted to single-layered individual microcolonies, which occasionally merge when founder cells fall relatively close to each other. To avoid boundary effects on microcolony growth under influence of a radial oxygen gradient (Fig. S2), we imaged microcolonies in a 3 mm^2 × 3 mm^2 area close to the patch center for consistency. Growth kinetic data of both species at different substrate concentrations show substrate limitation (see below), but we do not wish to claim that the patch center behavior is representative for all conditions of Ppu or Pve growth.

Since cells are tracked over time by imaging from the onset of the experiment (Fig. 1B), their apparent maximum specific growth rate can be calculated from the segmented colony area expansion during the exponential growth phase for each microcolony (Fig. 1C) under inclusion of local spatial positioning. To support the empirical observations of colony growth, we developed an accompanying model based on substrate diffusion, uptake, and utilization by spherocylindrical cell-agents with similar geometry as either Ppu or Pve cells (Fig. 1D). The model takes into account cell elongation, division, and cell–cell pushing during colony development, and recapitulated observed microcolony growth and spatial patterns (Fig. 1E). We then further used the model simulations to understand diffusive substrate-growth effects and the nature of emerging interactions in the observed mono- and coculture experiments (see below).

Microcolony growth rates as a function of added substrate concentration

In order to benchmark the system of surface colonization for Monod kinetics, we first examined the dependency of monoculture growth rates on increasing substrate concentrations. For this, we added succinate at increasing concentrations (0.01, 0.05, 0.5, 1, and 5 mM) and seeded cells of either Ppu or Pve individually, with a founder cell density per imaged area (ca. 1.7 × 10^4 μm^2) ranging from 30 to 70 cells for Ppu and from 30 to 150 cells for Pve. Fitted average colony expansion rates increased from 0 to 5 mM succinate, indicative for Monod-substrate dependency and suggesting carbon-limited growth (Fig. 2A). Both fitted average μ_{max} and K_S on succinate were higher for Ppu (1.01 h^{-1} and 0.018 mM, respectively), than for Pve (0.47 h^{-1} and 0.004 mM). Colony expansion rates did not decrease to zero in absence of any added succinate, indicating that both species can extract some carbon from the agarose medium (Fig. 2A; Fig. S3). By interpolating the fitted Monod curve, we estimated ca. 50 µM of succinate-equivalent carbon source to be available from the agarose. These results thus indicated that Ppu is the faster grower, but Pve potentially has a lower affinity for the substrate under the patch conditions.

To better understand the dynamics of substrate utilization by cells on the surface, we simulated Ppu growth at different cell seeding densities using the observed colony expansion rates at 1 mM succinate, and calculated the average remaining substrate concentrations in the agarose patch as a function of incubation

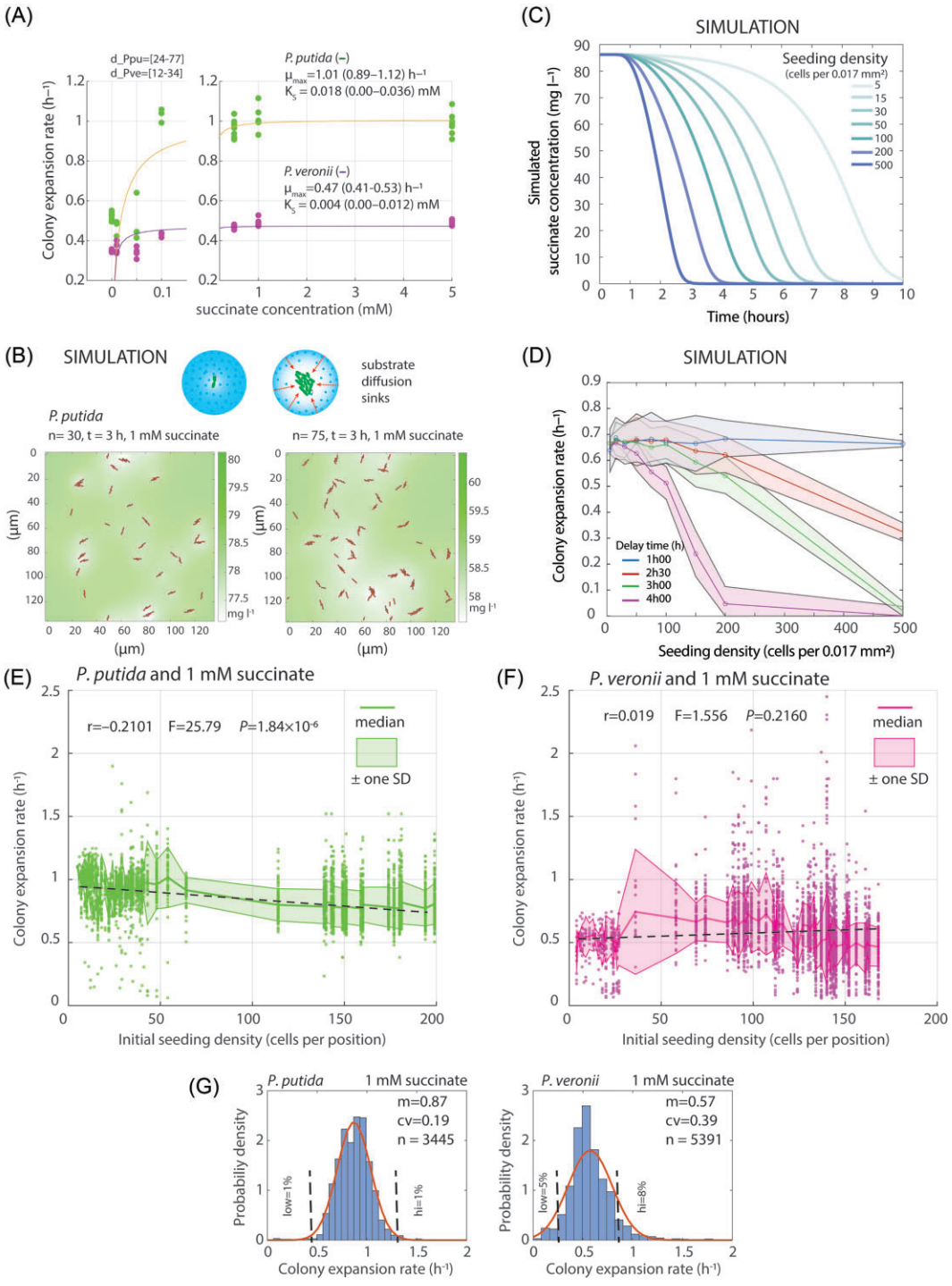

Figure 2. Growth kinetic properties of surface-grown Ppu or Pve founder cells. (A) Mean colony expansion rates of Ppu (green) or Pve (magenta) as a function of succinate concentration in the agarose disks. Circles, means of average expansion rates across image areas (d_PPU, d_PVE; range of observed seeding densities of founder cells). Lines and values show nonlinear Monod fitting. (B) Simulated substrate depletion as a function of incubation time and microcolony size in a virtual image area (134 μm^2 × 134 μm^2). Cells are shown in red (simulated sizes and orientations). Shades of green correspond to the simulated substrate concentration around the cells, according to the respective color scale on the right. (C) Average simulated substrate depletion times (starting from 1 mM succinate) as a function of cell seeding density (darker line color represents denser seeding as per the color scale). (D) Mean simulated colony expansion rates (solid lines) and their 95% confidence bounds (transparent colored zone) for the indicated starting cell densities after a predefined incubation interval (colors). Note how within 1 h (e.g. after depositing the cells and starting the imaging) one can expect to faithfully measure the maximum exponential colony expansion rate in the cell density range used for experiments here. (E) Effect of starting cell density (cells per image area position, ca. 0.017 mm^2) on the measured colony expansion rates of Ppu on 1 mM succinate. Solid line connects the median expansion rates within an image area, with green dots being the individual microcolony values and the transparent green zone denoting the median ± 1 SD. Statistics from linear regression on the means, testing the significance of difference to a zero slope (*r* is the Pearson correlation coefficient; *F* is the F-value; and *P* is the P-value). (F) As (E), but for Pve. (G) Distribution of colony expansion rates at 1 mM succinate for Ppu and Pve in monoculture conditions (six independent experiments). *n*, number of measured microcolonies; m, mean; and cv, coefficient of variation (mean μ/standard deviation). Vertical dashed lines indicate the mean ± 0.5 × the mean, to represent the proportion of colonies with outlier behavior (low and hi; in %).

time (Fig. 2B). This indicated, as expected, that the denser the amount of seeded cells on the surface, the faster the substrate is depleted (Fig. 2C). In other words, this would mean that at very high starting cell densities (>200 per image area), the time window to accurately measure the exponential growth rate after seeding the cells would be less than 2 h (Fig. 2D). In our further protocol, therefore, we targeted <150 seeded cells per unit of imaged area, and started the imaging maximally 30 min after seeding the cells. Based on these results, we used 1 mM succinate in the following experiments, which we concluded is not maximum growth rate-limiting and would permit substrate competition, while still restricting multilayered colony growth (as empirically observed).

In accordance with model predictions, the measured mean individual colony expansion rates at 1 mM succinate in six independent monoculture experiments remained relatively consistent across a range of starting cell densities (5–200 per imaging area of 0.017 mm^2). Ppu colony expansion rates decreased slightly but statistically significantly as function of increasing founder cell density (Fig. 2E; Pearson's coefficient $r = -0.2100$, $P = 1.84 \times 10^{-6}$), whereas those of Pve did not (Fig. 2F; $r = 0.0193$, $P = .2160$). The observed colony expansion rates at 1 mM succinate were less variable for Ppu ($n = 4$ experiments, mean = 0.87 h^{-1}, coefficient of variation = 0.19; Fig. 2G) than for Pve (0.57 h^{-1} and a coefficient of variation = 0.39), with 1% low and high Ppu microcolony outliers versus 5% and 8% for Pve (Fig. 2G; low and high defined as below or above the mean expansion rate ± 0.5 × the mean). As the substrate is homogenously present in the patches, this suggests an inherent phenotypic variability among founder cells, determining their reproductive success.

Growth kinetic heterogeneity among individual microcolonies

Despite different maximum specific colony expansion rates, all colonies in the imaged areas entered stationary phase at almost the same moment (visible from the arrest of colony area increase), whereby Ppu in mono-culture (Fig. 3A) reached stationary phase sooner than Pve (Fig. 3B; note that a further slow increase is detected at $t > 300$ min, which is due to continued expression of the fluorescent marker in nondividing Pve-cells that inflates the segmented colony area). Growth arrest of individual microcolonies is a consequence of one or more factors becoming growth-limiting. Their near-simultaneous stalling, despite being surrounded by appreciable empty space (Fig. 1E), suggests almost homogenous depletion of growth factors at the scale of the imaged areas. Therefore, even though larger colonies tend to locally deplete substrate concentrations (as indicated by simulations in Fig. 2B), molecular diffusion would rapidly counterbalance and equalize substrate concentrations at the imaged area scales (Fig. 2C). As a consequence of the near simultaneous growth cessation, the microcolonies reached different stationary phase sizes. The mean microcolony sizes for both Ppu and Pve decreased from 1 to 0.5 and 0 mM succinate (with same founder cell densities), as expected (Fig. 3C). Simulations showed, however, that individual microcolony sizes at stationary phase are largely dependent on the founder cell density (Fig. 3D and E), and their absolute sizes are, therefore, only of limited value to judge differences in biomass productivities as a result of interspecific interactions (such as substrate competition, for which we will introduce the species summed biomass ratio per unit of surface; see below).

To further understand the cause of colony size variability, we examined four possible factors: the number of neighbors at start, the apparent colony expansion rate, the lag phase of the founder cells (here taken as the time until first doubling of the initial cell area), and the area of available substrate intake [approximated by the Voronoi space at time of founder cell seeding, as described in Chacon et al. (2018)]. The number of nearby neighbors (scored as the number of neighboring founder cells in circles with increasing radii) correlated negatively with the final observed microcolony size, both for Ppu (Fig. 4A) and for Pve (Fig. 4B). Significant but weak correlations were found between the Voronoi area at start and the final attained microcolony areas for both Ppu and Pve (adjusted $R^2 = 0.405$ and 0.561, respectively, from a general linearized model; Fig. S4). However, there was no consistent correlation of the number of neighbors and the observed maximum colony expansion rates and a weak negative correlation of colony expansion rates at the highest neighbor densities at later growth stages (Spearman correlations; Fig. S5). This means that at the start, all founder cells perceive sufficient substrate influx to grow at maximum exponential rates. Most founder cells taken from exponentially growing precultures did not exhibit any apparent lag phase once they were deposited on the surface and the imaging had started, because their measured colony expansion rates were inversely proportional to the time of their first doubling (Fig. 4C and D; *expo*, exponential phase precultures). In contrast, Ppu founder cells prepared from stationary phase liquid suspended cultures showed ca. 10% of cells with a detectable longer lag phase than expected from their colony expansion rate (Fig. 4C, grey zone), whereas this was less than 1% for Pve (Fig. 4D). Interestingly, however, Ppu cells with longer lag times still displayed fast maximum growth rates. Collectively, these results indicated that the variable starting maximum growth rates of individual cells are predetermined at the time of seeding, perhaps as a consequence of preculturing history and cell phenotypic variability. Starting (maximum) growth rates of individual cells are not necessarily decreased by longer lag times.

As a consequence, stationary phase colony areas were not well explained from measured expansion rates (Fig. 4E; Spearman rank correlation coefficients –0.1701 and –0.0349, $P = .0041$ and .2700, respectively, for Ppu and Pve). That this is not a general rule is shown by cells taken from stationary phase precultures on succinate and seeded on surface without succinate (therefore only being able to profit from residual carbon in the agarose; Fig. 4F). In such case, the final microcolony sizes do correlate to the individual colony expansion rates (Fig. 4F; Spearman rank correlation coefficients of 0.6419 for Ppu and 0.3177 for Pve). In summary, variability in monoculture (maximum) growth rates of individual founder cells seems mostly predetermined by preculture conditions and phenotypic variation, whereas individual colony productivity (i.e. their stationary phase size) is to some extent dependent on the number of neighbors and the available substrate intake area, represented by the Voronoi space (Chacon et al. 2018). In addition, faster or bigger growing microcolonies may enhance their growth proportionally to others by locally depleting substrate faster, which biases further diffusion toward them and increases the net substrate flux into the colony.

Substrate competition in cocultures leads to growth rate reduction and local colony size effects

Having defined the range and variability of microcolony growth rates and yields in monocultures, we next quantified colony expansion parameters in cocultures of Ppu and Pve, in order to determine interaction effects. We first focused on conditions where we expected both species to engage in competition for the same

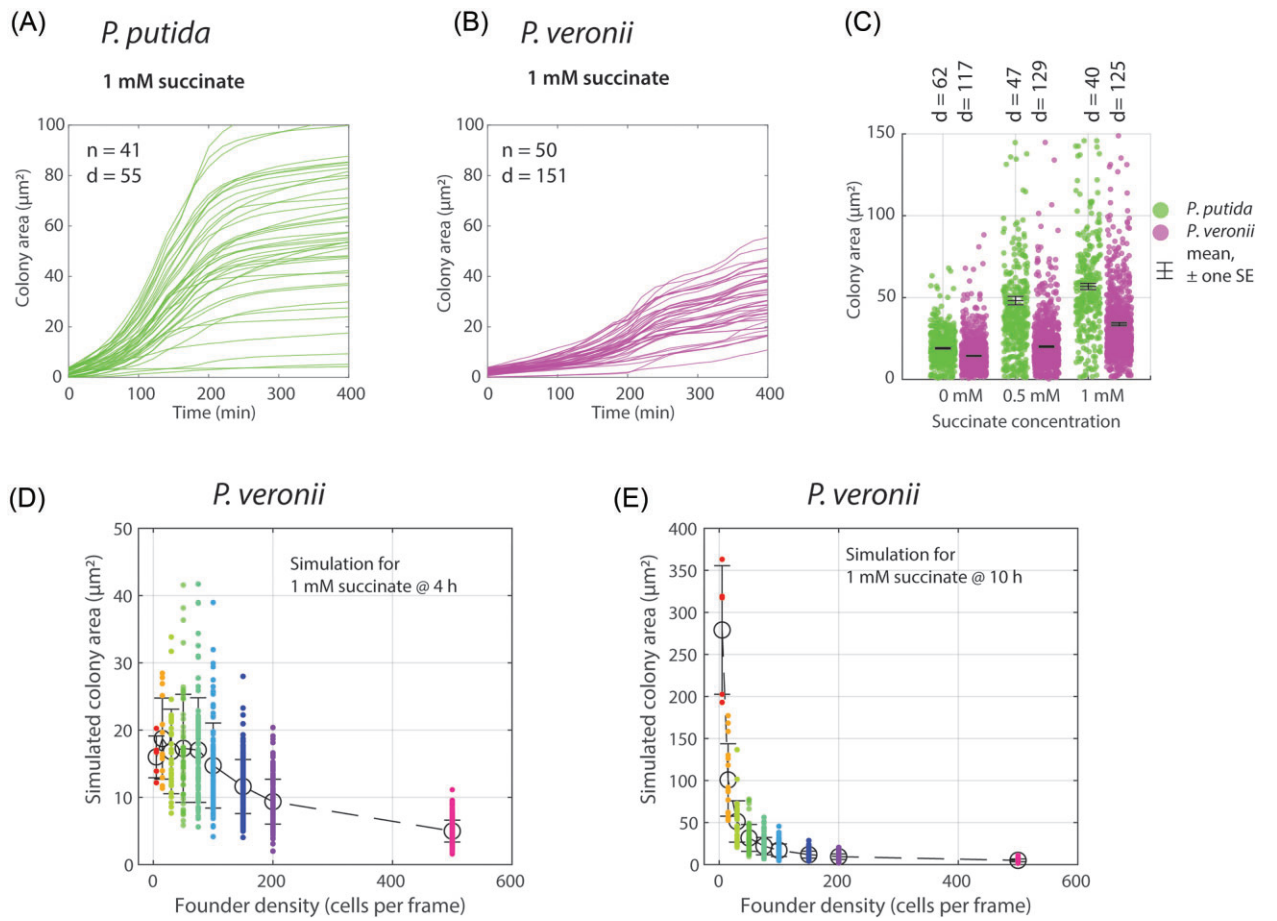

Figure 3. Microcolony productivity variation as a function of substrate concentration and founder cell density. (A) and (B) Microcolony growth and steady state area variation of Ppu (A) or Pve (B) with 1 mM succinate on a single imaged area as function of time, measured from area occupied by the fluorescent cells (as in Fig. 1B). Note how all colonies arrest growth at approximately the same time. *n*, number of colonies; d, founder cell density. (C) Observed microcolony size variability in stationary phase as a function of succinate concentration. Each dot is an individual microcolony, horizontal black bars indicate the mean ± 1 standard error (SE). d, mean founder cell density (cells per frame). (D) and (E) Simulated microcolony areas of Pve on 1 mM succinate after 4 h (D) and 10 h (E) as a function of founder cell density. Circles represent the mean of individual simulated microcolonies (colored dots), with bars representing ± 1 SD.

primary substrate (succinate). Since Ppu grows faster than Pve on succinate (Fig. 2E), our expectation here was that Ppu would outcompete Pve growth as seen in homogenous liquid cultures (Guex et al. 2023). Unexpectedly, microcolony expansion rates of both Ppu and Pve were lower in coculture than in monoculture, but coculturing had no or little effect on measured lag times (Fig. 5A). The coculture-dependent decrease of colony expansion rates was consistent across multiple different experiments, even at different succinate concentrations and seeding densities (Fig. S6), with an average decrease of 16.4% for Ppu and 14.9% for Pve (Fig. 5B; $n = 10$ and 8, and *P*-values of 6.39×10^{-5} and .0026, respectively, from unpaired two-sided *t*-tests). Individual microcolonies of either strain at the same seeding density grew on average to smaller size in co- than in corresponding monocultures (Fig. S7). In terms of global productivity (e.g. summed stationary phase colony size for each of the strains per imaged area position), Pve lost 90% in coculture with Ppu compared to monoculture, whereas Ppu lost on average 27% (Fig. 5C). There was no significant difference in summed productivity of both species in coculture and that of Ppu in monoculture ($P = .1776$; Fig. 5C). If we define the competitive loss factor on growth rate for Ppu as the relative difference compared to monoculture growth, this then equalled 1–0.164 = 0.836 and on productivity 1–0.27 = 0.73, whereas that of Pve equalled 1–0.149 = 0.871 on growth rate and 1–0.90 = 0.10 on productivity. Cell counts measured by flow cytometry across the whole patch at stationary phase showed similar competitive loss for Pve in the coculture compared to its monocultures (0.10; Fig. 5D), but no significant difference for Ppu productivity in the mixture compared to its monocultures ($P = .3075$, $n = 10$). This difference between bulk and patch center measurements is possibly the result of higher replicate variation in the cocultures (Fig. 5D) or of boundary growth effects (Fig. S2) that are taken into account in quantification of the agarose-surface washed cell suspension but not by the microscopy measurements.

To estimate competition at a local scale, we compared the number and summed microcolony areas of either species surrounded by colonies of itself or of the other species, in circles of increasing radius, for each detected microcolony (Fig. 5E). This procedure captures local differences in seeding densities and ratios, which can be used to calculate and plot the relation between the species ratio at start and their final biomass ratio (Fig. 5E). In case of equally competitive strains for the same substrate, one would expect the slope of the starting species ratio and their final biomass ratio to be equal to 1, since the summed biomass yield (*X*) per unit of surface would remain the same and will be divided proportionally by either species based on its founder cells (Fig. 5E, slope line).

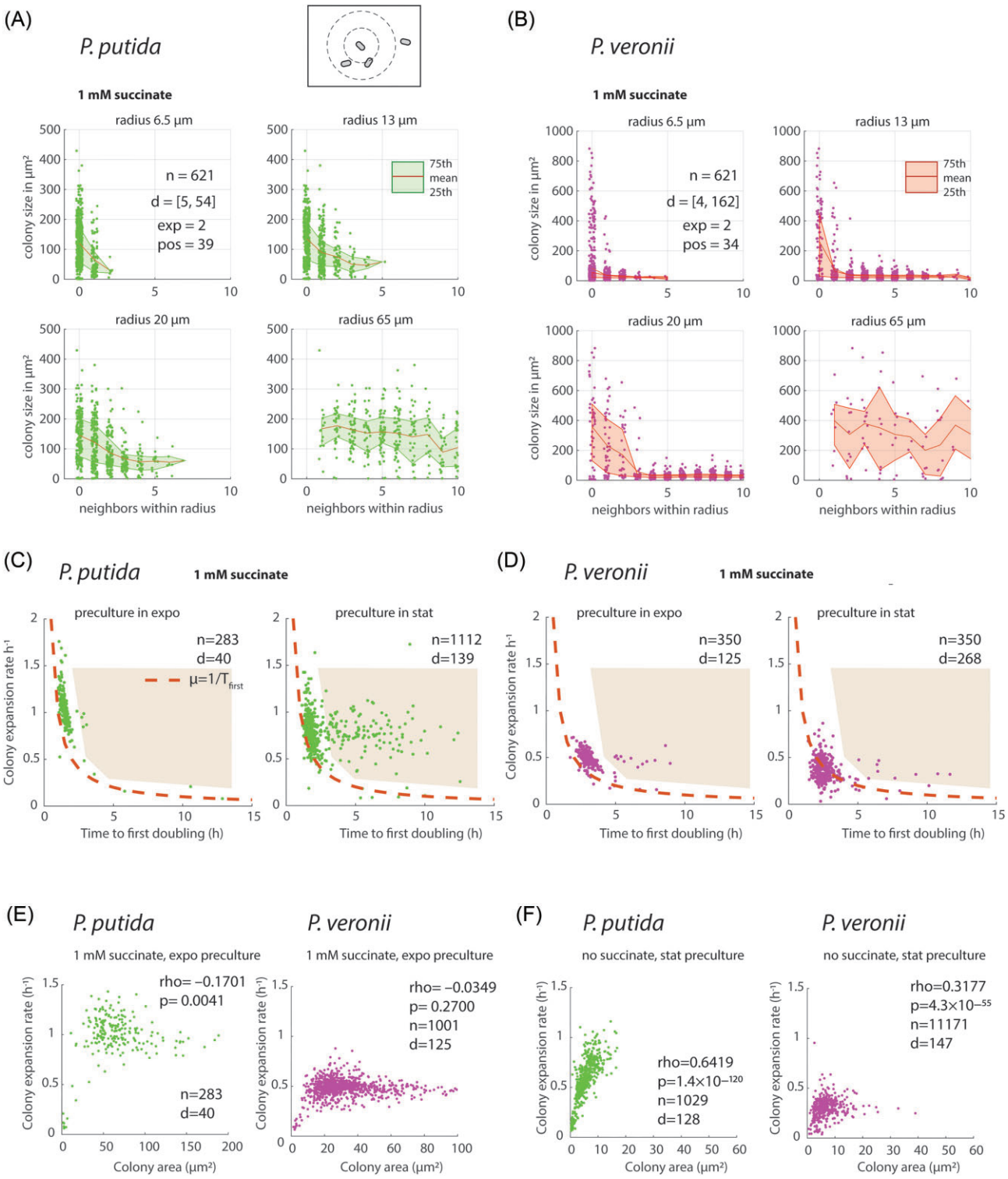

Figure 4. Dependencies of microcolony growth properties on available surface area. (A) and (B) Relationship between attained colony areas (individual dots) and area occupation by neighboring kin, calculated as the number of colonies within a circle of diameter 6.5, 13, 20, or 65 µm around each cell (as depicted in the cartoon). Colony data from patches with 1 mM succinate in monoculture. *n*, number of plotted microcolonies; d, range of founder cell densities; exp, number of independent experiments, and pos, imaged positions. Red lines connect the means with the color transparent zone bounding the 25th–75th percentile range. (C) and (D) Relationship between measured colony expansion rate and the time to first doubling (as the sum of the fitted lag time and the inverse of the measured colony expansion rate) for Ppu (C) or Pve (D) monocultures on 1 mM succinate, seeded either from exponentially growing precultures (expo), or stationary phase cultures (stat). *n*, number of microcolonies in the plotted datasets (Pve subsampled to 350); d, mean founder cell density per image area. Dotted line shows the expected time to first doubling without lag phase (as 1/colony expansion rate). Shaded areas are manually added to highlight cells with extended lag times. (E) and (F) Stationary phase colony areas as a function of measured colony expansion rates for Ppu or Pve at 1 mM succinate, with precultures from exponential phase (E) on the same substrate, or from stationary phase cultures seeded on patches without succinate added (F). rho, Spearman correlation coefficient; *P*, corresponding *P*-value for the Spearman correlation.

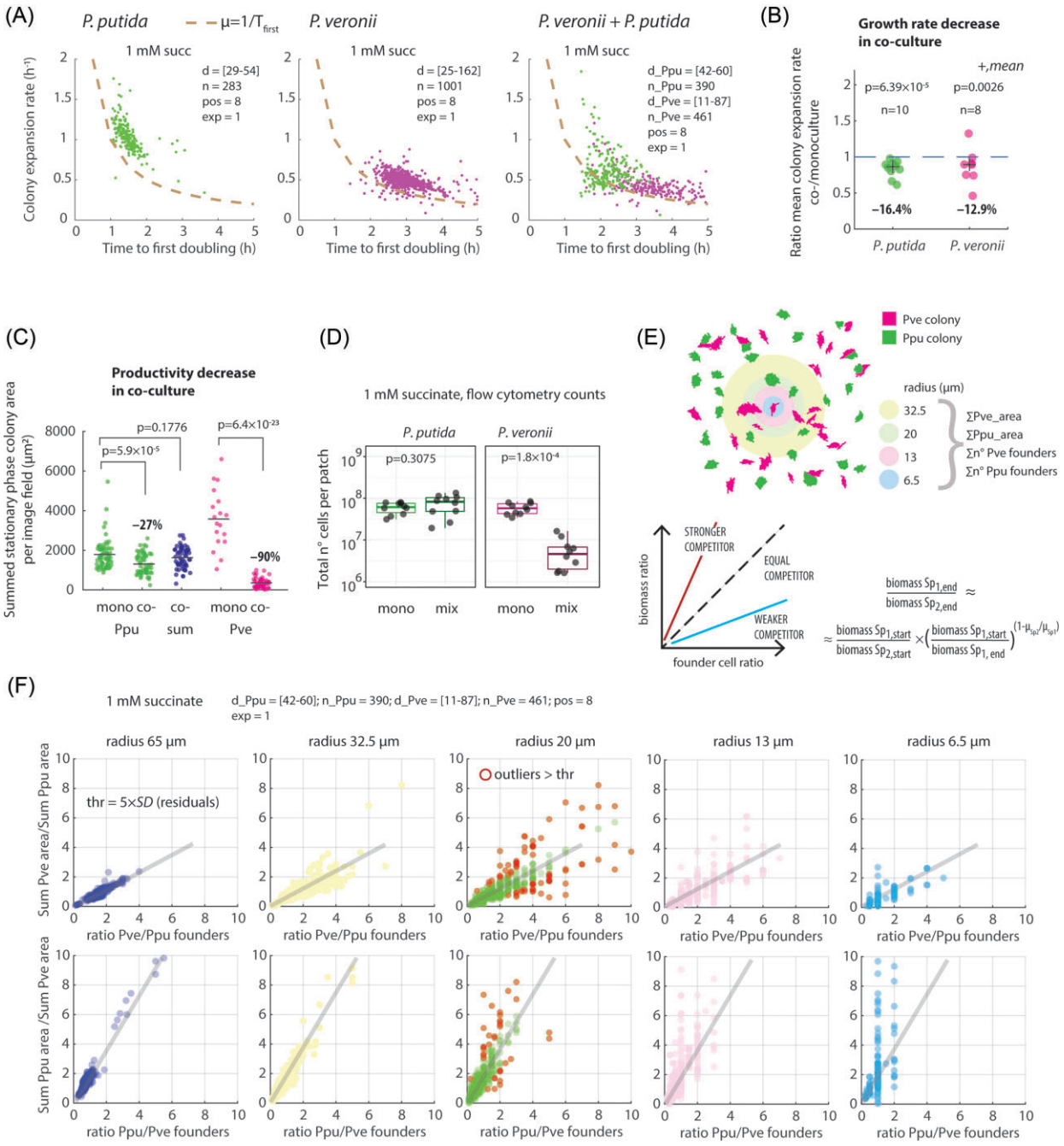

Figure 5. Interspecific interactions from microcolony growth properties of cocultured Ppu and Pve on a single competing substrate. (A) Colony expansion rates for Ppu (green dots) or Pve (magenta) in monoculture, or in coculture on 1 mM succinate, as a function of time to first doubling (h; being the inverse of the measured colony expansion rate plus fitted lag time). Dotted lines show the expected inverse relation of growth rate and time to first doubling in absence of lag time. Precultures were taken from exponential phase on the same substrate. d, density range of seeded founder cells; *n*, pos, exp, number of microcolonies, imaged positions, and experiments, respectively. (B) Difference of mean microcolony expansion rates in coculture compared to monoculture (*n*, number of experiments; *P*-values from unpaired two-sided *t*-testing). (C) Productivity decrease in coculture compared to monoculture, taken as the sum of microcolony stationary phase areas per imaged field. Dots represent technical replicates (image fields) across experiments with the same succinate concentration. *P*-values from unpaired two-sided *t*-testing. Co-sum, per image field summed areas of both Ppu and Pve. (D) Total number of cells on patches of mono- or cocultures, grown with 1 mM succinate, determined by flow cytometry of washed suspensions. (E) Principle of quantifying local neighbor competition. The number and colony areas of neighboring self or nonkin microcolonies (based on the geometric center at the first image frame) are quantified within circles of increasing radii (here represented by different colors) around each individual detected microcolony (either Ppu—green; or Pve—magenta). This is used to calculate and plot the ratio of summed species colony areas (biomass ratio) as a function of the ratio of the founder cell numbers. In case of equal competitors, one would expect a slope of 1. The equation indicates the theoretical relation for logistic coculture growth (Sp, species). (F) Derived local neighborhood competition, shown here for a single experiment example (all experiments shown in Fig. S8) of coculture growth with 1 mM succinate for the five circle radii, either from Pve (top row), or the inverse Ppu microcolony perspective (bottom row). Seeding densities (d_PPU and d_PVE), total number of microcolonies (n_PPU and n_PVE) and number of imaged positions (pos) reported on top. Colors correspond to circle radii of panel (E). The slope line of the linear regression at the circle radius of 65 μm is used to define the residual variation and 5× the standard deviation of the residuals is used as a threshold (thr) to identify the proportion of outlier colonies at the neighborhood radius of 20 μm (red circles, as reported in Table 1). Slope lines from 65-μm radius are reproduced on the other diagrams for clarity.

Table 1. Local competitive interaction parameters.

Comparison	Substrate	Simulation or experiment	Mean interaction slope[d]	Inverse interaction slope	Mean outliers up[e]	Mean outliers down[e]	Proportion local competition overturn[f]
Ppu versus Pve	Succinate	Cross-feeding[a]	2.78	0.36	0.0079	0.1058	
	Succinate	Direct competition[a]	2.93	0.34	0.0310	0.0959	
	Succinate	No variation[a]	2.24	0.45	0	0	
	Succinate	1 mM[b]	1.95 ± 0.118	0.51	0.021 ± 0.013	0.055 ± 0.023	
	Putrescine and D-mannitol	Two substrates[a]	0.74	1.56	0.125	0.121	
	Putrescine and D-mannitol	1 + 0.6 mM[c]	0.348	2.87	0.015	0.257	
Pve versus Ppu	Succinate	Cross-feeding[a]	0.347	2.88	0.095	0.204	
	Succinate	Direct competition[a]	0.426	2.37	0.218	0.142	
	Succinate	No variation[a]	0.407	2.46	0	0.008	
	Succinate	1 mM[b]	0.559 ± 0.06	1.789	0.145 ± 0.025	0.071 ± 0.037	0.130 ± 0.018
	Putrescine and D-mannitol	Two substrates[a]	3.84	0.260	0.301	0.077	
	Putrescine and D-mannitol	1 + 0.6 mM[c]	3.19	0.313	0.182	0.127	

[a] $n = 5$ simulations, each with seeding density of 49 Pve + 51 Ppu cells per simulated image area.
[b] $n = 4$ experimental data sets combined.
[c] $n = 1$ experiment with four imaged positions.
[d] Linear regression as in Fig. 5(E), for the 20-µm radius calculation; inverse is 1/slope.
[e] Proportion of points with residual values for the 20-µm radius calculation >3 × standard deviation to the regression line and its variation at radius 65 µm. For example, *down* outliers in the Ppu versus Pve comparison refer to cases where Pve grows better than expected.
[f] Defined as Pve colonies within 20-µm radius with summed colony area more than that of Ppu, corrected for founder cell ratio.

In other words, the term in Fig. 5(E) $(X_{Sp_{1,start}})/(X_{Sp_{2,start}})^{(1-\mu_{Sp^2}/\mu_{Sp^1})} = 1$ at identical maximum growth rates.

Analysis of the slope lines for different circle diameters (Fig. 5F; Fig. S8) showed two interesting aspects: (i) the slopes remained almost constant for neighborhood circles from large to small, although individual variation increased, and (ii) the slopes for the final biomass ratio/founder cell ratio relationships from Pve perspective were almost perfectly inverted to those from Ppu perspective (Fig. 5F, Table 1; Table S2). The analysis thus captures the expected competitive interaction with Ppu being the stronger and Pve the weaker competitor on succinate, and even at the smallest neighborhood scale of 6.5 µm radius. When assuming that the global relation is best captured by the largest circle radius (65 µm; Fig. 5F), one can use the variation of the residuals on the linear regression slope to set a threshold (here: 3 × SD, or 99.5% likelihood), above which an individual microcolony would behave statistically differently than the global trend. We applied this criterium for the circle radius of 20 µm, which indicated, for example, that 14.5% of Pve microcolonies locally grow bigger than expected from the competitive interaction (or 5.5% from the perspective of Ppu microcolonies, Table 1). In 13% of the local Pve microcolonies within 20-µm circle radius, their collective biomass ratio to that of Ppu surpasses a value of 1, indicating they would locally overturn the competition to their favor (Table 1).

Characterizing the Ppu–Pve interaction under conditions with exclusive substrates

To place the effect of primary substrate competition into perspective, we repeated the same experiment, but with an exclusive substrate for each of the species such that they would become indifferent for each other. The best combination to achieve this and which abolished competition in liquid culture (albeit not perfect) used putrescine as selective substrate for Ppu and D-mannitol for Pve (Guex et al. 2023). Despite the intended independence, some 10% of Pve colonies showed diauxic growth, indicating they may be able to use putrescine (at a later stage; Fig. 6A). As intended, the productivity of both species on the combination of putrescine and D-mannitol in coculture was less drastically affected (Fig. 6B; loss factors 0.61 and 0.67 for Ppu and Pve, respectively) than with succinate (0.73 and 0.10; Fig. 5E), although in this substrate combination the summed stationary phase productivity in the coculture was less than the sum of the monoculture productivities (Fig. 6B). This indicates that also under substrate independence conditions both species do not grow completely independently from each other. Individual maximum growth rates observed for Ppu (taken at the first 4 h) were on average 2-fold increased in presence of Pve (Fig. 6C and D), but no different for Pve in presence or absence of Ppu (Fig. 6D). In presence of Ppu, however, the variability among growth rates of Pve microcolonies increased (Fig. 6C). Local competition analysis by the ratio of founder cells to the ratio of final biomasses indicated a reversal of the slope lines for Pve and Ppu (Fig. 6E), which was again robust for different neighborhood scales (Fig. 6E and F). In contrast to what was observed for succinate, Pve was the stronger competitor (slope of 3.19) than Ppu (slope of 0.348) on putrescine and D-mannitol (Table 1).

Surface coculture growth simulations underscore metabolite-driven interactions

To better understand the potential causes of observed coculture effects on kinetics of microcolony growth, we simulated different interspecific interaction scenarios (Supplementary data simulations). Coculture simulations were started with randomly placed founder cells of either species or else with starting positions matching those of the experiments. Cells of either species were given growth kinetic properties based on their monoculture experimental values, plus a random variation equal to the observed standard deviation. We did not exhaustively investigate parameter space effects, but concentrated on simulating a number of potential credible scenarios (Fig. 7A). Direct competition for

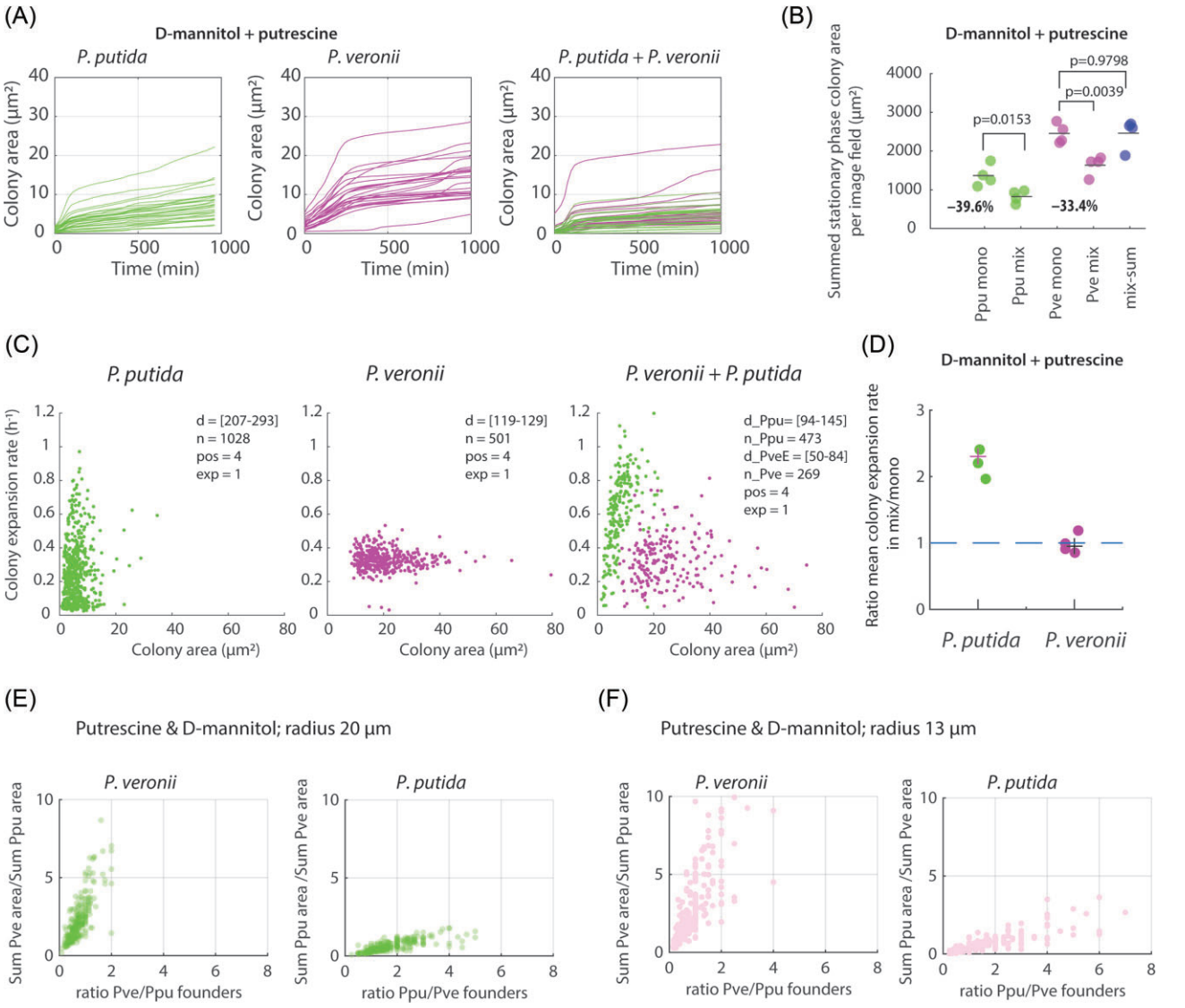

Figure 6. Coculture behavior under substrate independence conditions. (A) Microcolony growth of Ppu or Pve separately or in mixture on D-mannitol and putrescine. Only the first increase is used to calculate the maximum specific growth rate (i.e. typically between 0 and 200 min). (B) Stationary phase productivity difference in mono- or coculture growth (productivity is the sum of microcolony areas per image field, here as individual dots). P-values from two-sided unpaired *t*-testing ($n = 4$). (C) Colony expansion rates as a function of stationary phase colony area. (D) Ratio of mean growth rates in co- versus monoculture for either Ppu (PPU) or Pve. Local neighborhood competition of Pve and Ppu on putrescine and D-mannitol as ratio of founder cells and final colony biomass area ratio in a 20-µm (E) or 13-µm radius neighborhood (F). Colors correspond to circle radii in Fig. 5(E). Note the reversal of the slopes in comparison to succinate (Fig. 5F). Slope values reported in Table 1.

the single added substrate (succinate), was not able to explain the observed reduction in growth rates; neither was a simulation scenario with sharing of the same metabolites (Fig. 7B). In contrast, simulating both cross-feeding (i.e. production and uptake of different metabolites) or cross-feeding with interspecific inhibition resulted in a reduction in growth rates of both species (Fig. 7B). As expected, all scenarios predicted a lower productivity of Pve compared to Ppu, and all but direct substrate competition caused a reduction in the normalized productivity sum (Fig. 7C). Inclusion of a mutual inhibition resulted in the largest reduction in the productivity sum (Fig. 7C). Also, the relation of founder cell ratios to final biomass ratios across all experiments with 1 mM succinate (slope = 1.76) was better explained by the cross-feeding (slope = 2.16) than by the direct competition scenario (slope = 2.60; Fig. 7D; $n = 5$ simulations for three founder cell ratios each). These values are close to the values obtained for the 20-µm neighborhood radii as in Table 1, and this indicates that the surface competitive interaction on succinate is decreased by 1–1.76/2.60 = 0.32 for Ppu and increased by 2.60/1.76–1 = 0.48 for Pve, compared to what would be expected from monoculture growth rate and yield differences alone (i.e. direct competition scenario).

The variation of simulated individual colony sizes and their maximum expansion rates for the cross-feeding and inhibition scenarios captured the main trends observed in the experimental data, both for succinate and for the mixture of putrescine and D-mannitol (Fig. 7E). However, removing from the simulations either the variation in maximum growth kinetics or variation in lag phase of starting cells, yielded much less variation in colony expansion rates, which is not in agreement with experimental observations (Fig. 7E). This underscores, therefore, the crucial effect of inherent differences in growth kinetic properties of founder cells on the productivity of their microcolony descendants.

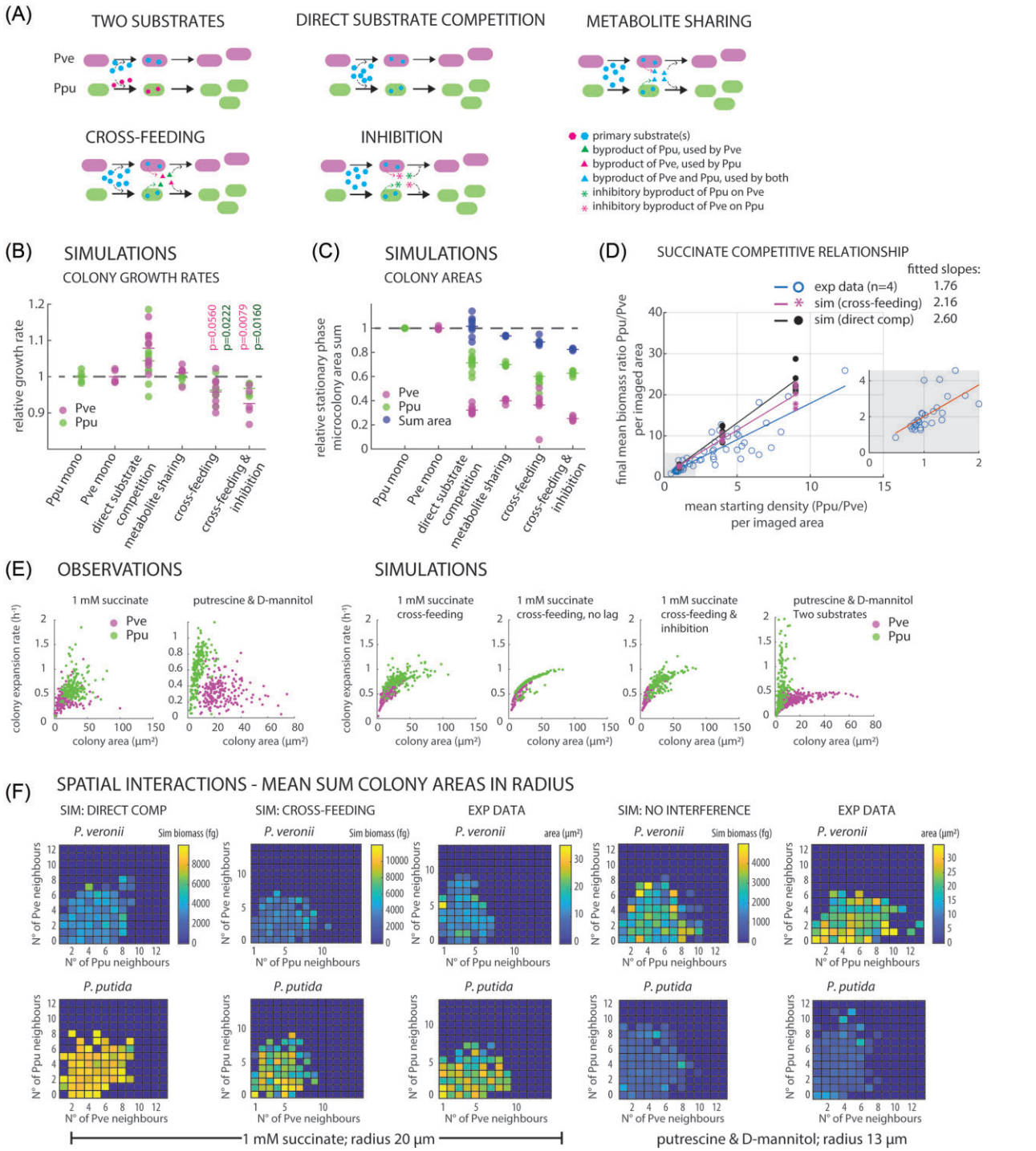

Figure 7. Simulated interaction scenarios explain reduced growth rates in cocultures. (A) Different tested scenarios of cross-feeding or inhibition between Ppu and Pve. (B) Relative growth rates of either Ppu or Pve in competition scenarios compared to their monoculture simulations ($n = 5$–7 simulations; Supplementary data simulations). P-values correspond to unpaired t-tests between co- and monoculture simulation replicates. (C) as (B), but for the final attained microcolony area sum (per simulated image field). Sum area, sum of Pve and Ppu colony areas in that simulated image field. (D) Comparison of empirical local neighborhoud competition at 1 mM succinate ($n = 4$ experiments) with cross-feeding and direct substrate competition simulations ($n = 5$ simulations, each with 3 starting ratios). Data points are the ratio of the mean starting density ratio of Ppu/Pve per imaged area and their final mean biomass ratio (summed microcolony areas). Slope lines and values from linear regression are indicated. Inset shows region of founder cell ratio below 2 (i.e. where Pve is more abundant). (E) Comparison of observed (1 mM succinate and putrescine and D-mannitol) final colony areas versus colony expansion rates of Pve and Ppu in coculture, and four simulation conditions, as indicated and explained in panel (A). (F) Effect of spatial densities of self and nonkin neighboring microcolonies on the mean summed colony areas within a radius of 20 µm (1 mM succinate) or 13 µm (putrescine and D-mannitol, due to the higher seeding density in this experiment). Mean summed colony areas as function of neighbor density is shown as heatmap according to the provided color scale, either from the perspective of Pve microcolonies (top row; simulations in fg biomass, experiments in µm² area) or Ppu (bottom row). Plots compare three simulation interaction scenarios (SIM, as explained in panel A), and two experimental data set (EXP). Note how the cross-feeding simulation better represents the experimental data for succinate than the direct competition scenario. Also, note the slight benefit of Ppu to grow better with few Ppu but Pve neighbors in case of succinate (and *vice versa*), and the positive effect of Ppu neighbors but few Pve neighbors on Pve growth, and of Ppu growth with Pve but no other Ppu neighbors with putrescine and D-mannitol.

Finally, we explored whether interactions would show as local variations of final colony areas as a function of the density of neighboring kin or nonkin colonies, assuming that, for example, cross-feeding might only be detectable if a colony of one species would be surrounded by few nonkin but not kin colonies. Direct competition would generally predict no local effects of kin and nonkin density differences (Fig. 7F, Fig. S9), although it captures the strong excess of Ppu compared to Pve growth on succinate. In contrast, the cross-feeding scenario predicts a slightly higher Ppu biomass when locally few other Ppu but twice as many (4–7) Pve colonies are present. In experimental data, we detect slightly larger Ppu colonies with no or one Ppu neighbors, and one neighboring Pve colony. Overall, however, the variation of colony area distributions as a function of neighbors in experimental data looks more similar to the cross-feeding than the direct competition simulations. For the case of two substrates we observed general positive influence of Ppu neighbors around few Pve colonies (one or two), and *vice versa* (slightly higher Ppu colony areas in absence of neighboring Ppu but in presence of few Pve neighbors in the same area, Fig. 7F; Fig. S9). This was not captured by the two substrate simulations for the independence scenario (Fig. 7F), and indicates that both species are indeed not growing completely orthogonal on the two substrates.

Extensive production and sharing of metabolites in competition

To support the suggestion that differential metabolite production and uptake can determine interaction outcomes, we repeated Ppu and Pve mono- and coculture growth in liquid suspension to facilitate targeted metabolomics analysis. No significant effects on Ppu or Pve growth rates could be detected after swapping their (exponential phase) culture medium to that of the other species (Fig. 8A; Fig. S10), although Pve with Ppu-supernatant showed a shorter delay in resuming growth (Fig. S10). The excreted metabolites in pure cultures were very similar among both species, and all accumulated over time, except dihydrouracil (Fig. 8B). Ppu notably produced higher peak areas (here taken as a proxy for concentrations) of (5′-)deoxyadenosine, *cis*-aconitate and homocysteine than Pve, whereas Pve produced more alpha-ketoglutarate, cyclic-GMP, ethanolamine, *N*-acetylputrescine, and salicylate than Ppu (Fig. 8B). The sum of the peak areas of the produced metabolites accounted for 25.4% of the initial succinate concentration (in peak area) for Ppu, and 23.5% for Pve. Despite a number of obvious differences in mono-culture metabolite production, both Ppu and Pve showed very few significant differences in the utilization and production of metabolites starting from their own exponential phase supernatant or from that of the other species (Fig. 8C). At a cutoff of 2-fold difference and adjusted *P*-value of .05, only Ppu produced more cyclic-GMP, deoxyguanosine, *N*-acetyl leucine, and thymidine with Pve's supernatant than with its own (Fig. 8C). These results thus indicated that both Ppu and Pve produce very similar metabolites, but can reciprocally reutilize those, which are specifically produced by the other species.

Discussion

We successfully showed that a simple microcolony growth platform can be expanded from mono- (Eijlander and Kuipers 2013, Koutsoumanis and Lianou 2013, Nghe et al. 2013, Jung and Lee 2016, Sankaran et al. 2019) to cocultures to parametrize growth kinetic and interspecific interaction effects. Similar setups to study paired interactions are so far extremely rare (Niggli et al. 2021, Laffont et al. 2024), but, as we demonstrate, have a high potential for producing rich data sets that encompass both individual and local variability as well as global growth interaction effects. In that sense, the microcolony platform is versatile, quantitative and extrapolates across scales (Fig. 5F). The platform is easily adaptable to different growth conditions or spatial heterogeneities, and can potentially be scaled to higher order mixed cultures by colony phenotypic recognition (Marcoux et al. 2014, Paquin et al. 2022, Doh et al. 2023) instead of genetically encoded fluorescence to differentiate the strains.

How well does the microcolony platform capture and scale the imposed interaction effects (substrate competition and independence)? The loss of individual biomass formation for Ppu or Pve under substrate competition in co- compared to monocultures as observed for the entire patch-population (e.g. Fig. 5D) was similar to that measured previously in liquid suspended cultures (Guex et al. 2023). As expected from its higher maximum specific growth rate on succinate, Ppu globally outcompeted Pve both for surface- and liquid grown cocultures. The dominance of Ppu over Pve, and the loss of individual biomass in cocultures was also reflected in the decrease of global mean individual stationary phase microcolony areas (Fig. S5), the summed colony areas per image field (Fig. 5C), and in the relation between final species biomass ratios and founder cell ratios (Fig. 5F). Especially the biomass to founder cell ratio analysis was consistent to local neighborhoods as small as 13 µm in diameter, which accentuated more the individual variation. The individual variation is largely dependent on random positioning, general seeding density effects (Fig. 3D and E; Fig. S4), and the phenotypic variation of founder cells (Fig. 4E and F). At local scales, we find that the competitive disadvantage for Pve can be overturned, and the stochastic positioning and founder cell phenotypic variations can result in better than expected Pve microcolony growth (e.g. outlier definitions in Fig. 5F and Table 1). The frequency of overturned competitive effects is low (ca. 13%) but non-negligible (Table 1), and may contribute to a better than expected proliferation of poorer competing species in a spatial context.

A more unexpected finding with the microcolony coculturing platform was the consistent measured decrease in maximum specific growth rates of both Ppu and Pve by ca. 15% in surface-grown cocultures compared to monocultures at the same seeding densities (Fig. 5A and B). This is not *a priori* expected from Monod-theory, which dictates that maximum specific growth rates should be solely dependent on prevailing substrate concentrations, which we showed here (Fig. 2) are not limiting for both Ppu and Pve, at least not during the duration for measuring the colony expansion rates. The decrease in maximum specific growth rates in coculture under succinate competition is consistent with the differences in measured slope of the founder cell ratio to final biomass ratio and theoretical competition (Fig. 7D), indicating that competitive interactions have an additional component not captured by inherent mono-culture growth kinetic differences. Our control experiment to generate independence growth conditions indeed alleviated the observed reduction in growth rates (Fig. 6D) and inversed the interaction behavior between the strains (Fig. 6E), but was not completely orthogonal since both strains lost some biomass production in co- versus monocultures (Fig. 6B).

The question remains as to the mechanism underlying growth rate reductions under competition. Model simulations with the coculture agent-based model suggested that neither primary substrate competition nor metabolite sharing can explain maximum growth rate reduction (Fig. 7B). The only two likely scenarios that could yield growth rate and biomass reduction are the

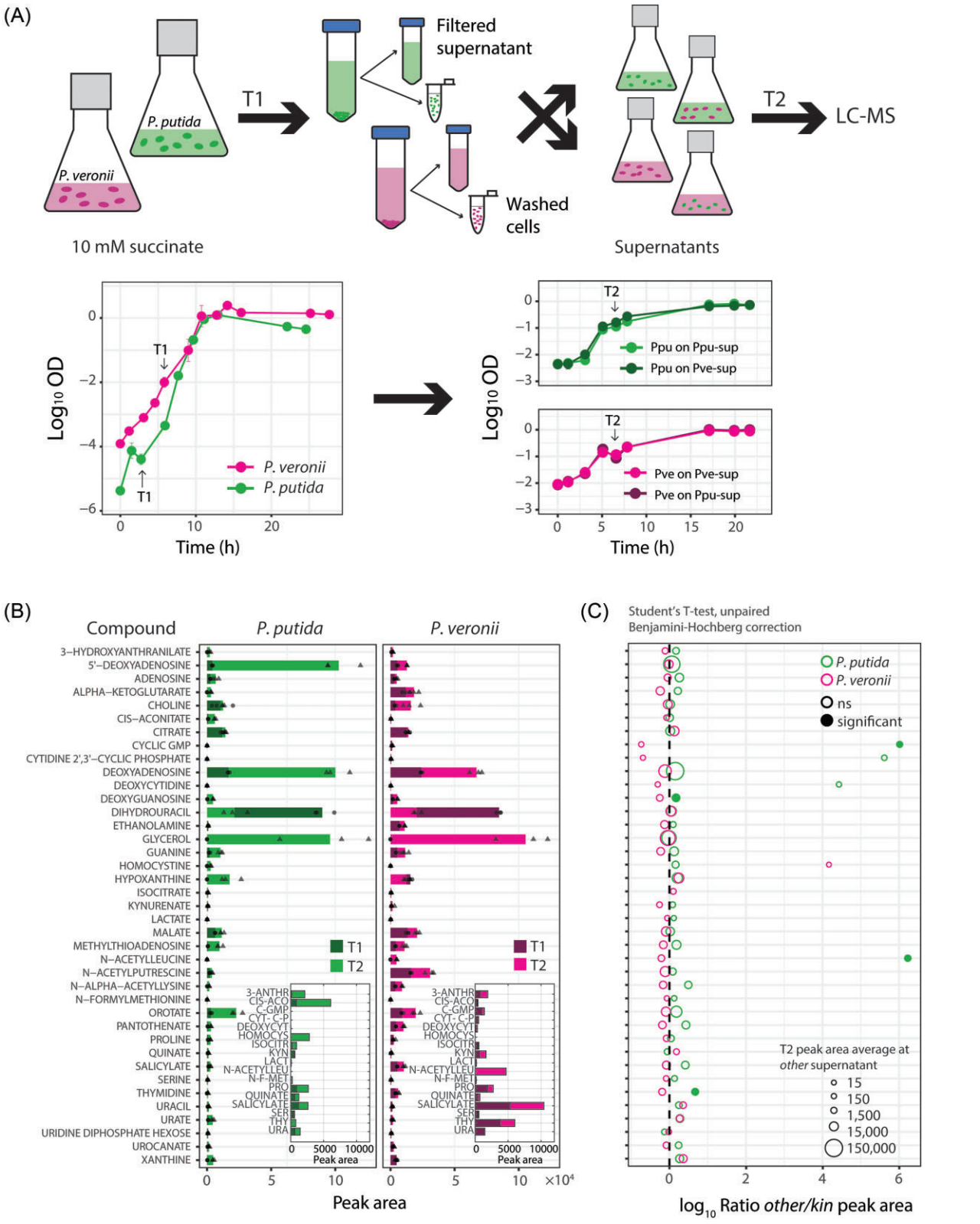

Figure 8. Exometabolite analysis of growing mono- and cocultures. (A) Growth of Ppu and Pve in monocultures on 10 mM succinate and on reciprocal cell-free supernatants harvested from exponential cultures of either strain (for more detailed time series and growth rate determinations, see Fig. S6). Dots represent the means of independent biological triplicates. T1, T2: sampling and swapping times. (B) Targeted detected metabolites in monoculture supernatants of either strain in exponential (T1) and early stationary phase (T2). Bars show the mean detected peak area from biological triplicates, with circles (for T1) and triangles (for T2) showing individual values. Inset repeats low abundance compounds on different scale. (C) Log_{10} ratio of the compounds' T2 areas in incubations of the *other* species' and its own supernatant (*kin*). Significance of difference by paired *t*-test corrected for multiple testing (as filled circles at $P < .05$).

production of some nonkin-targeted inhibitor compound, the utilization of a major metabolite that is not used by the producer strain, or a combination of both (Fig. 7B and C). Indeed, the LC–MS targeted analysis confirmed that both strains, as assumed more in general for growing bacterial cultures (Goldford et al. 2018, Pacheco et al. 2019) are rather leaky, and efflux a large variety of (similar) metabolites during exponential growth. By analysing mono- and coculture swapped supernatants of the strains grown in liquid suspension, we found one compound which is exclusively formed by Ppu but not accumulating in Pve cultures (5′-deoxyadenosine; Fig. 8B and C), and a few minor ones for the reciprocal direction (e.g. c-GMP, *N*-acetylputrescine). Notably, 5′-deoxyadenosine is a side-product of biotin formation, which was shown to be an inhibitor for *Escherichia coli* in absence of a deoxyadenosine-cleaving nucleosidase (Choi-Rhee and Cronan 2005), whereas also 2′,3′-cyclic nucleotide monophosphates are reported to have physiological and signaling effects (Marotta and Weinert 2023). Suspected inhibitory effects on growth rates, however, could not be recapitulated by liquid suspended culturing of either strain in reciprocal exponential phase cell-free supernatant. We can, therefore, neither confirm nor refute the inhibition hypothesis, which would require testing of individual compounds from the exometabolites on species growth. In addition, some effects may be specific for the dynamic spatial setting of growing microcolonies and difficult to recapitulate in liquid cocultures.

The underlying context for compound-diffusible interactions to emerge is that monoculture growth constitutes a combination of direct substrate metabolism leading to new cell biosynthesis, and conversion of substrate to intermediates. Some of those leak out but then are taken up again either by the cells of their own kin, or by subpopulations of cells with different physiology (Dal Co et al. 2019) or by neighboring species (Hansen et al. 2007). Mathematically speaking, this can be approached by a summation of multiple growth rates that combine into a single maximum specific growth rate (Supplementary data simulations). In a spatial setting, the efflux of metabolic intermediates would lead to microcolonies becoming net producers and effectively losing carbon through radial diffusion, from which nearby other competing species may profit, as suggested earlier (Guex et al. 2023). Metabolic exchange has been seen before for a binary couple of engineered amino acid auxotrophies in *E. coli* under microfluidic growth (Dal Co et al. 2020), but our data suggest that this should be a much more general phenomenon. Local variation in microcolony and individual cell physiologies, seeding densities, and species starting ratios can then lead to local deviation of global interaction effects (as in Figs 5E, F, and 7F).

The agarose patch platform reflects the dynamic nutrient situation for most bacteria in natural habitats. As example, by seeding cells on the agarose surface in a closed microscope chamber as presented here, with glass slides touching either surface, population growth not only results in carbon source depletion but potentially also in reduction of the radial oxygen diffusion rate. For the two strains that we use; Ppu as an obligate aerobic bacterium and Pve as a facultative denitrifier, this may result in more profuse Ppu growth near the patch edges (Fig. S2), temporarily lowering the oxygen diffusion to the patch center. For consistency of the measurements across the different experiments we only focused on microcolony growth in the patch center, but by exploiting the differences in locally measured interactions at positions along the patch cross-section, one could characterize the dynamic nature of the emerging interactions in a broader spatial context. Also, by embedding local or solid substrate sources or including heterogenous obstacles for diffusion in the patch, one could better describe the effects of spatial nutrient context, formation of gradients, substrate flow and diffusion, or substrate dissolution—either chemically or through activities of other microorganisms.

In conclusion, the direct quantification of growth kinetic parameters from surface-grown microcolonies in mono- and coculture permits detecting global as well as local interaction effects, which can be used to describe the effects of interspecific interactions on growth in a spatial context. The robust capturing of interaction effects even at small local scales would permit studying the types and variations of emerging interactions from surface growth of more species-diverse communities in real-time. The microcolony growth platform is thus a useful expansion to transduce scales in community growth behavior and link to physiological theory.

Acknowledgments

We thank Simon van Vliet for helpful critical comments on the manuscript. We are very grateful to Victor de Lorenzo, Leo Eberl, Paul Rainey, and Yuya Karita for their critical input and reviewing of our work.

Author contributions

T.M.T., M.D., I.G., C.M., and J.M. conceived the studies and designed experiments. T.M.T., M.D., and E.S-L. conducted microcolony growth experiments. I.G. and C.M. developed the surface-growth cell-agent based model. I.G. scripted the model code, and I.G. and J.M. performed model simulations. X.R. and H.T. conceived the microcolony image analysis and codes. T.M.T., M.D., and J.M. analysed microcolony data. T.M.T., I.G., and J.M. analysed output data, and wrote the draft manuscript. All authors gave input, verified, and corrected the written manuscript. C.M. and J.M. acquired funding and coordinated the work.

Supplementary data

Supplementary data is available at *FEMSML Journal* online.

Conflict of interest: The authors declare no competing interests.

Funding

This work was supported by the Swiss National Science Foundation (Sinergia program, grant CRSII5 189919/1 to J.M. and C.M.), SystemsX.ch grant 2013/158 (Design and Systems Biology of Functional Microbial Landscapes “MicroScapesX” to J.M.), and by the National Centre in Competence Research (NCCR) in Microbiomes (grant number 180575 to J.M.).

Data availability

All data and code of the surface agent-based growth model (MATLAB), of the colony image segmentation (Python), and data processing of imaging and other results (R, MATLAB) is available from a single download at Zenodo (Miguel Trabajo et al. 2024).

References

Angeles-Martinez L, Hatzimanikatis V. Spatio-temporal modeling of the crowding conditions and metabolic variability in microbial communities. *PLoS Comput Biol* 2021;**17**:e1009140.

Basler M, Ho BT, Mekalanos JJ. Tit-for-tat: type VI secretion system counterattack during bacterial cell-cell interactions. *Cell* 2013;**152**:884–94.

Bickel S, Or D. Aqueous habitats and carbon inputs shape the microscale geography and interaction ranges of soil bacteria. *Commun Biol* 2023;**6**:322.

Borer B, Ciccarese D, Johnson D *et al.* Spatial organization in microbial range expansion emerges from trophic dependencies and successful lineages. *Commun Biol* 2020;**3**:685.

Chacon JM, Mobius W, Harcombe WR. The spatial and metabolic basis of colony size variation. *ISME J* 2018;**12**:669–80.

Choi-Rhee E, Cronan JE. A nucleosidase required for in vivo function of the S-adenosyl-L-methionine radical enzyme, biotin synthase. *Chem Biol* 2005;**12**:589–93.

Coyte KZ, Schluter J, Foster KR. The ecology of the microbiome: networks, competition, and stability. *Science* 2015;**350**:663–6.

Dal Bello M, Lee H, Goyal A *et al.* Resource-diversity relationships in bacterial communities reflect the network structure of microbial metabolism. *Nat Ecol Evol* 2021;**5**:1424–34.

Dal Co A, van Vliet S, Ackermann M. Emergent microscale gradients give rise to metabolic cross-feeding and antibiotic tolerance in clonal bacterial populations. *Philos Trans R Soc Lond B Biol Sci* 2019;**374**:20190080.

Dal Co A, Van Vliet S, Kiviet DJ *et al.* Short-range interactions govern the dynamics and functions of microbial communities. *Nat Ecol Evol* 2020;**4**:366–75.

Doh IJ, Zuniga DVS, Shin S *et al.* Bacterial colony phenotyping with hyperspectral elastic light scattering patterns. *Sensors* 2023;**23**:3485.

Eijlander RT, Kuipers OP. Live-cell imaging tool optimization to study gene expression levels and dynamics in single cells of *Bacillus cereus*. *Appl Environ Microbiol* 2013;**79**:5643–51.

Emmenegger B, Massoni J, Pestalozzi CM *et al.* Identifying microbiota community patterns important for plant protection using synthetic communities and machine learning. *Nat Commun* 2023;**14**:7983.

Faust K, Raes J. Microbial interactions: from networks to models. *Nat Rev* 2012;**10**:538–50.

Gerhardt P, Murray RGE, Costilow RN *et al. Manual of Methods for General Bacteriology*. Washington, DC: American Society for Microbiology, 1981.

Goldford JE, Lu N, Bajic D *et al.* Emergent simplicity in microbial community assembly. *Science* 2018;**361**:469–74.

Goldschmidt F, Regoes RR, Johnson DR. Successive range expansion promotes diversity and accelerates evolution in spatially structured microbial populations. *ISME J* 2017;**11**:2112–23.

Guex I, Mazza C, Dubey M *et al.* Regulated bacterial interaction networks: a mathematical framework to describe competitive growth under inclusion of metabolite cross-feeding. *PLoS Comput Biol* 2023;**19**:e1011402.

Hansen SK, Rainey PB, Haagensen JA *et al.* Evolution of species interactions in a biofilm community. *Nature* 2007;**445**:533–6.

Jung JH, Lee JE. Real-time bacterial microcolony counting using on-chip microscopy. *Sci Rep* 2016;**6**:21473.

Kehe J, Ortiz A, Kulesa A *et al.* Positive interactions are common among culturable bacteria. *Sci Adv* 2021;**7**:eabi7159.

Koutsoumanis KP, Lianou A. Stochasticity in colonial growth dynamics of individual bacterial cells. *Appl Environ Microbiol* 2013;**79**:2294–301.

Laffont C, Wechsler T, Kümmerli R. Interactions between *Pseudomonas aeruginosa* and six opportunistic pathogens cover a broad spectrum from mutualism to antagonism. *Environ Microbiol Rep* 2024; **16**:e70015. https://doi.org/2024.03.22.586229.

Liao C, Wang T, Maslov S *et al.* Modeling microbial cross-feeding at intermediate scale portrays community dynamics and species coexistence. *PLoS Comput Biol* 2020;**16**:e1008135.

Marcoux PR, Dupoy M, Cuer A *et al.* Optical forward-scattering for identification of bacteria within microcolonies. *Appl Microbiol Biotechnol* 2014;**98**:2243–54.

Marotta NJ, Weinert EE. Insights into the metabolism, signaling, and physiological effects of 2',3'-cyclic nucleotide monophosphates in bacteria. *Crit Rev Biochem Mol Biol* 2023;**58**:118–31.

Martinez-Garcia E, Calles B, Arevalo-Rodriguez M *et al.* pBAM1: an all-synthetic genetic tool for analysis and construction of complex bacterial phenotypes. *BMC Microbiol* 2011;**11**:38.

Miguel Trabajo T, Guex I, van der Meer JR. Dataset and scripts belonging to "Inferring Bacterial Interspecific Interactions from Microcolony Growth Expansion". Zenodo, 2024. https://doi.org/10.5281/zenodo.13284638.

Momeni B, Brileya KA, Fields MW *et al.* Strong inter-population cooperation leads to partner intermixing in microbial communities. *eLife* 2013;**2**:e00230.

Morales M, Sentchilo V, Bertelli C *et al.* The genome of the toluene-degrading *Pseudomonas veronii* strain 1YdBTEX2 and its differential gene expression in contaminated sand. *PLoS One* 2016;**11**:e0165850.

Nestor E, Toledano G, Friedman J. Interactions between culturable bacteria are predicted by individual species' growth. *mSystems* 2023;**8**:e0083622.

Nghe P, Boulineau S, Gude S *et al.* Microfabricated polyacrylamide devices for the controlled culture of growing cells and developing organisms. *PLoS One* 2013;**8**:e75537.

Niggli S, Wechsler T, Kummerli R. Single-cell imaging reveals that *Staphylococcus aureus* is highly competitive against *Pseudomonas aeruginosa* on surfaces. *Front Cell Infect Microbiol* 2021;**11**:733991.

Pacheco AR, Moel M, Segre D. Costless metabolic secretions as drivers of interspecies interactions in microbial ecosystems. *Nat Commun* 2019;**10**:103.

Pacheco AR, Pauvert C, Kishore D *et al.* Toward FAIR representations of microbial interactions. *mSystems* 2022;**7**:e0065922.

Paquin P, Durmort C, Paulus C *et al.* Spatio-temporal based deep learning for rapid detection and identification of bacterial colonies through lens-free microscopy time-lapses. *PLOS Digit Health* 2022;**1**:e0000122.

Piccardi P, Vessman B, Mitri S. Toxicity drives facilitation between 4 bacterial species. *Proc Natl Acad Sci* 2019;**116**:15979–84.

Rainey PB, Rainey K. Evolution of cooperation and conflict in experimental bacterial populations. *Nature* 2003;**425**:72–4.

Raynaud X, Nunan N. Spatial ecology of bacteria at the microscale in soil. *PLoS One* 2014;**9**:e87217.

Reinhard F, van der Meer JR. Life history analysis of integrative and conjugative element activation in growing microcolonies of *Pseudomonas*. *J Bacteriol* 2014;**196**:1425–34.

Reinhard F, van der Meer JR. Microcolony growth assays. In: Timmis KN, de Lorenzo V, McGenity T, van der Meer JR (eds), *Handbook of Hydrocarbon and Lipid Microbiology*. Vol. **5**. Berlin, Heidelberg: Springer, 2010, 3562–70.

Rochat L, Pechy-Tarr M, Baehler E *et al.* Combination of fluorescent reporters for simultaneous monitoring of root colonization and antifungal gene expression by a biocontrol pseudomonad on cereals with flow cytometry. *Mol Plant Microbe Interact* 2010;**23**:949–61.

Rodríguez Amor D, Dal Bello M. Bottom-up approaches to synthetic cooperation in microbial communities. *Life* 2019;**9**:22.

Sankaran J, Tan N, But KP *et al.* Single microcolony diffusion analysis in *Pseudomonas aeruginosa* biofilms. *npj Biofilms Microbiomes* 2019;**5**:35.

Schäfer M, Pacheco AR, Kunzler R *et al.* Metabolic interaction models recapitulate leaf microbiota ecology. *Science* 2023;**381**:eadf5121.

Sentchilo VS, Zehnder AJB, van der Meer JR. Characterization of two alternative promoters and a transcription regulator for integrase expression in the *clc* catabolic genomic island of *Pseudomonas* sp. strain B13. *Mol Microbiol* 2003;**49**:93–104.

Tecon R, Or D. Biophysical processes supporting the diversity of microbial life in soil. *FEMS Microbiol Rev* 2017;**41**:599–623.

van den Berg NI, Machado D, Santos S *et al.* Ecological modelling approaches for predicting emergent properties in microbial communities. *Nat Ecol Evol* 2022;**6**:855–65.

Widder S, Zhao J, Carmody LA *et al.* Association of bacterial community types, functional microbial processes and lung disease in cystic fibrosis airways. *ISME J* 2022;**16**:905–14.

Zelezniak A, Andrejev S, Ponomarova O *et al.* Metabolic dependencies drive species co-occurrence in diverse microbial communities. *Proc Natl Acad Sci USA* 2015;**112**:6449–54.

Zylstra GJ, Gibson DT. Toluene degradation by *Pseudomonas putida* F1. *J Biol Chem* 1989;**264**:14940–6.

Received 16 September 2024; **accepted** 3 October 2024